Structural Durability & Health Monitoring

Tech Science Press

Doi:10.32604/sdhm.2025.064902

ARTICLE

Energy Dissipation and Stiffness Assessment: A Study on RC Frame Joints Reinforced with UHPSFRC

Trung-Hieu Tran*

Faculty of Civil Engineering, Hanoi Architectural University, Hanoi, 100000, Vietnam

*Corresponding Author: Trung-Hieu Tran. Email: hieutt@hau.edu.vn

Received: 27 February 2025; Accepted: 24 April 2025; Published: 30 June 2025

ABSTRACT: The design principles for conventional reinforced concrete structures have gradually transitioned to seismic-resistant design since the 1970s. However, until recently, the implementation of strength capacity and ductility design has not been rigorously enforced in many developing countries that are prone to seismic risks. Numerous studies have evaluated the effectiveness of joint behavior based on both ductile and non-ductile designs under cyclic loading. Previous research has demonstrated that enhancing joint regions with Ultra-High Performance Steel Fiber Reinforced Concrete (UHPSFRC) significantly improves the seismic resistance of structural components. This paper presents a detailed analysis of the considerable improvements in energy dissipation capacity and stiffness degradation observed in both reinforced test samples compared to the control sample. Furthermore, assessing the effective performance of enhanced reinforced concrete joints is a critical parameter for evaluating the feasibility of this approach. The findings highlight the potential for UHPSFRC to enhance the resilience of concrete structures under seismic loads, providing a viable solution to improve the safety and durability of infrastructure in earthquake-prone regions. This study aims to inform future design methodologies and standards in seismic-resistant construction in developing nations, emphasizing the importance of adopting innovative materials to mitigate earthquake risks effectively.

KEYWORDS: Ultra-high-performance concrete (UHPC); exterior joint; reversed cyclic loading; energy dissipation capacity; stiffness degradation

1 Introduction

The field of reinforced concrete (RC) structural engineering has witnessed a paradigm shift since the 1970s, transitioning from conventional design principles to a more rigorous seismic-resistant design philosophy. This evolution acknowledges the inherent vulnerability of RC structures to seismic events and emphasizes the need for designs that can effectively withstand and dissipate the energy associated with earthquake ground motions. While significant progress has been made in developing sophisticated analytical models and design methodologies that incorporate inelastic behavior, challenges remain in fully capturing the complexities of RC structural response, especially in regions prone to seismic activity. Many developing nations, often facing budgetary constraints and infrastructural limitations, have not yet fully adopted these advanced seismic design practices, highlighting a critical need for robust and readily implementable solutions that enhance the seismic resilience of existing and future RC structures.

The development of high-performance concrete (HPC) and, more recently, ultra-high-performance concrete (UHPC) represents a significant advancement in concrete technology. The compressive strength of conventional concrete, typically ranging from 60 to 80 MPa in the 1970s [1], has been substantially improved

through innovative material science and manufacturing techniques. The evolution from conventional concrete to HPC involved a systematic reduction of the water-cement ratio, typically from 0.6 to 0.4, resulting in a significant decrease in porosity and enhanced strength characteristics [2–4]. This refinement, complemented by the introduction of superplasticizers to improve workability, has led to compressive strengths in HPC exceeding 100 MPa and even reaching values significantly higher than 200 MPa in certain specialized applications [5–8]. Recent studies have further advanced this field by exploring the integration of UHPC with steel fibers to form Ultra-High Performance Steel Fiber Reinforced Concrete (UHPSFRC), offering a unique combination of strength, ductility, and energy dissipation capacity that is particularly suited for seismic applications [9]. The novelty of this study lies in its focused investigation of UHPSFRC's application in RC frame joints, an area where existing research has predominantly concentrated on global structural behavior rather than localized joint enhancement under cyclic loading [10]. While the structural behavior of RC frame joints reinforced with UHPSFRC has been widely studied, the specific contribution of UHPSFRC to joint shear behavior, stiffness degradation, and energy dissipation under reversed cyclic loading remains underexplored, particularly in the context of developing countries with limited seismic design enforcement [11]. This paper addresses these gaps by providing a detailed experimental analysis of UHPSFRC-reinforced joints, highlighting their potential to offer a cost-effective and practical solution for seismic retrofitting.

The next step in this evolution has been the development and application of ultra-high-performance steel fiber-reinforced concrete (UHPSFRC). This advanced material combines the exceptional strength and durability of UHPC with the enhanced ductility and energy dissipation properties afforded by the incorporation of high-performance steel fibers. The judicious dispersion of these fibers within the UHPC matrix leads to a composite material exhibiting superior tensile strength, improved fracture toughness, and enhanced resistance to crack propagation. These properties make UHPSFRC particularly well-suited for applications where high strength and resilience are paramount, such as in seismic-resistant design. UHPC, and its fiber-reinforced counterpart, has already found widespread use in demanding structural applications worldwide, including high-speed railway tracks, airport runways, bridges, and even specialized military infrastructure [12]. Notable examples include the runways at Haneda Airport in Tokyo, the Gärtnerplatz Bridge in Kassel, Germany, toll booths for the Millau Viaduct in France, and various other high-profile projects [12]. The use of steel fibers in UHPSFRC often eliminates the need for conventional reinforcing steel in certain applications, further streamlining construction and potentially reducing costs. Moreover, recent research has demonstrated that UHPSFRC can significantly enhance the performance of RC structural elements, particularly in joint regions, where high stress concentrations occur during seismic events [13]. For instance, studies have shown that UHPSFRC improves the shear capacity and ductility of beam-column joints, yet the precise mechanisms of stiffness degradation and energy dissipation under cyclic loading require further clarification [14]. This study builds on these findings by systematically evaluating these parameters, offering new insights into the practical implementation of UHPSFRC in seismic-prone regions.

The behavior of reinforced concrete frame joints, both conventional and those enhanced with advanced materials, has been the subject of extensive research for over six decades. A comprehensive understanding of joint behavior is crucial for predicting the overall seismic performance of RC structures. Several key parameters significantly influence the shear capacity of these joints, including concrete compressive strength (f_c'), joint detailing and configuration, axial load effects, the geometric aspect ratio (typically represented as the ratio of beam height to column height, hb/hc), and the amount of reinforcement provided. Despite extensive research, a complete understanding of the interactive effects of all these parameters remains elusive. The complexity of the problem, coupled with variations in design codes, testing protocols, and the inherent challenges associated with conducting large-scale experimental programs, has hampered the development

of universally applicable design guidelines. To address this, the material properties of UHPSFRC used in this study were tested in accordance with ASTM C39/C39M for compressive strength and ASTM C1609/C1609M for tensile strength and ductility, ensuring reliable and standardized results [15,16]. These tests revealed exceptional mechanical properties, which were critical to the observed performance improvements in the joint regions. Recent literature has also emphasized the need for more detailed experimental data on UHPSFRC-reinforced joints, particularly under realistic seismic loading conditions [17–19]. For example, comparisons with studies on hybrid fiber-reinforced UHPC show that steel fibers alone can achieve comparable ductility with reduced material costs, underscoring the practical significance of this approach [20].

Further complicating the matter is the difficulty in accurately measuring and modeling the influence of axial loads on the behavior of the joints. Moreover, precise measurement of joint shear deformation has been reported only in a limited number of research studies [21–23], and there is a lack of consensus regarding the most appropriate methods for characterizing joint behavior under different loading conditions. Recent studies have highlighted the significance of the limit state defined by the onset of the initial diagonal crack in the joint region, emphasizing its strong influence on the overall shear deformation [22,24]. Most experimental research to date has focused on planar frames subjected to cyclic loading, while comprehensive testing of three-dimensional frame joints under biaxial loading conditions remains limited due to the complexity of such testing and the availability of specialized equipment. Furthermore, critical aspects like energy dissipation capacity, stiffness degradation, and the overall effectiveness of the joint are often underrepresented in current research findings. This study aims to bridge these knowledge gaps by providing a detailed investigation of UHPSFRC-reinforced joints, with a particular focus on their enhanced performance under reversed cyclic loading, an area where recent advancements in material science have yet to be fully exploited [25]. The motivation for this research stems from the urgent need to develop innovative, accessible solutions for seismic retrofitting in developing nations, where conventional methods may be impractical due to resource constraints [26]. By leveraging the superior properties of UHPSFRC, this study not only advances the understanding of joint behavior but also proposes a scalable approach to improve the seismic resilience of RC structures worldwide.

2 Testing Program

2.1 Specimen Design and Fabrication

Under lateral loading, inertial forces are transferred between stories via the columns. In most cases, columns experience approximately equal and opposite bending moments at their ends, resulting in zero moment points at mid-height (Fig. 1). Consequently, the analysis of the test specimens focuses on sections located at mid-column height and mid-span of the beams.

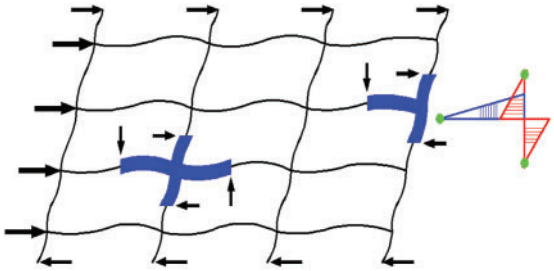

Figure 1: Frame under lateral load

This study employed three reinforced concrete (RC) joint specimens, meticulously designed and fabricated to investigate the influence of UHPSFRC on joint shear behavior. These specimens, designated S1, S2, and S3, were subjected to rigorous cyclic loading tests to assess their performance under simulated seismic conditions. The design aimed to isolate the effect of UHPSFRC enhancement on the joint's capacity for energy dissipation and stiffness degradation while controlling other variables.

Specimen S1 served as the control specimen, representing a conventionally reinforced RC joint. Its dimensions were precisely controlled at 350 mm × 450 mm, encompassing both the beam and column sections that constitute the joint. The longitudinal reinforcement consisted of a combination of 2D25 and 2D20 bars, strategically placed to provide sufficient tensile and compressive strength. Furthermore, transverse reinforcement, in the form of 10 mm diameter ties, were incorporated at 100 mm spacing within the joint region and at 200 mm spacing in the beam sections external to the joint. This arrangement of transverse reinforcement aimed to provide adequate confinement to the concrete core and mitigate the effects of tensile cracking and shear stresses within the joint area.

Specimens S2 and S3 were designed to directly assess the impact of UHPSFRC enhancement on joint performance. These specimens mirrored the dimensions and longitudinal reinforcement of the control specimen (S1) to isolate the effect of the UHPSFRC. The critical difference lay in the incorporation of UHPSFRC layers within the joint region, replacing the conventional concrete. Specimen S2 featured an 800 mm thick layer of UHPSFRC, while specimen S3 incorporated a thicker 1025 mm layer. UHPSFRC layers maintained a consistent cross-sectional area of 350 mm × 350 mm. A crucial aspect of the design for S2 and S3 was the intentional omission of the conventional transverse reinforcement within the UHPSFRC-enhanced zone. This omission aimed to isolate the contribution of the UHPSFRC to confinement and ductility, minimizing confounding effects from the presence of traditional transverse reinforcement.

Outside the joint region, the column sections of all three specimens were reinforced consistently with 10D20 longitudinal bars and transverse reinforcement, using 80 mm tie spacing for S2 and 100 mm spacing for S1 and S3. This consistent reinforcement in the column regions ensured consistent confinement in this area, helping isolate the effects of the UHPSFRC within the joint itself. Fig. 2 provides a detailed schematic illustrating the dimensions and reinforcement details of all three specimens. Table 1 below summarizes the key design parameters for each specimen, facilitating direct comparison and analysis of the results. This meticulous design approach ensured a controlled experimental environment, maximizing the validity and reliability of the conclusions drawn from the subsequent cyclic loading tests. The mechanical properties of materials used are provided in Table 2. The mix proportions of the conventional concrete and UHPSFRC used are presented in Table 3.

The UHPC employed in this study exhibited a high compressive strength of 122.93 MPa, coupled with a direct tensile strength of 8.1 MPa and a modulus of elasticity of 41,946 MPa. These properties, alongside a Poisson's ratio of 0.2, indicate the material's exceptional strength and stiffness, characteristics which are essential for enhancing the seismic resilience of reinforced concrete structures. The measured mechanical properties align with typical values reported for high-performance UHPC, suggesting that the material selection successfully balanced strength, stiffness and ductility requirements for the intended application. The high strength-to-weight ratio of the UHPC made it a suitable material choice for the study given the requirements for the experimental tests.

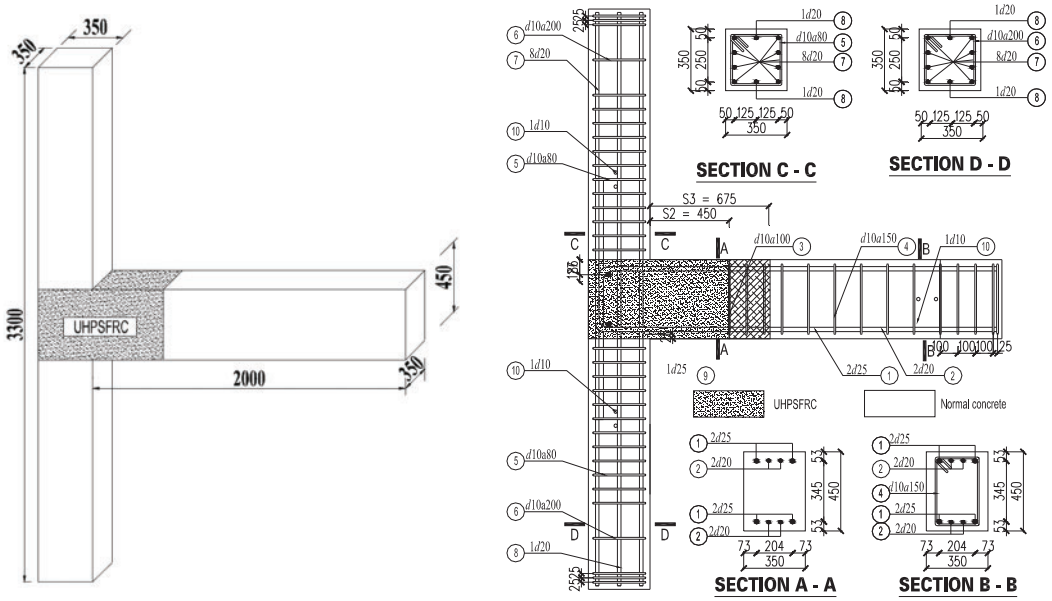

Figure 2: Geometric dimensions of the test specimen (Unit: mm)

Table 1: Detailed design of the test specimens

	Specimen	S1	S2	S3
Beam	Section (mm)		350 × 450	
	Longitudinal reinforcement		2d25 + 2d20	
	Stirrups	d10a100	*Critical zone* d10a100	–
		d10a150	*Out of critical zone* d10a150	d10a150
	Enhanced regional distance (mm)	–	800	1025
Column	Section (mm)		350 × 350	
	Longitudinal reinforcement		10d20	
	Stirrups		Critical zone: d10a80 Out of critical zone d10a200	
Joint zone	Vertical force (kN)		650	
	Stirrups (mm)	6 legged *d*10*a*80	–	–

Table 2: Mechanical properties of materials

Reinforcement					
	Diameter (mm)	**Cross-sectional area (mm²)**	**Yield strength (MPa)**	**Ultimate strength (MPa)**	**Modulus (GPa)**
Longitudinal beam and column reinforcement	10	50	585	701	200
Stirrups	20	314	577	695	200
Longitudinal column reinforcement	25	491	528	662	200
Steel fiber					
Diameter (mm)	Lengh (mm)	Lengh/diameter	Density (g/cm³)	Tensile strength (MPa)	Modulus (GPa)
0.2	13.0	65.0	7.9	2500	200
Concrete					
Concrete compressive strength at 28 days (MPa)			58.38		

Table 3: Mix proportions of the conventional concrete and UHPSFRC

Material quantity per m³ (kg)								
	Fiber content	**Water**	**Cement**	**Silica fume**	**Quartz sand**	**Superplasticizer (%)**	**Gravel**	**Limestone powder**
Normal concrete	–	190	450	–	824	1.2	893	225
UHPSFRC	2%	162	886	222	1109	39.5	–	–

The fabrication of the RC joint specimens (S1, S2, and S3) was conducted horizontally at a 1:1 scale using 20 mm thick film-coated plywood formwork to ensure a smooth surface and ease of construction. To prevent water leakage during casting, gaps between wooden formwork panels were sealed with waterproof adhesive, and 50 mm aluminum bars were used to connect the formwork sides, providing stability against concrete pressure. Steel reinforcement cages were assembled by fixing longitudinal bars to stirrups, with intermediate stirrups in the joint region tied to stabilize the longitudinal bars, and beam cages were positioned perpendicular to column cages in the joint area. Conventional concrete was mixed at a batching plant and cast outside the enhanced joint zones, while UHPSFRC, prepared in the laboratory with mix proportions as per Table 3, was cast within the joint regions (800 mm for S2 and 1025 mm for S3), separated by wooden dividers to avoid mixing, which were removed post-casting to ensure monolithic integrity. After 24 h, specimens were demolded and cured under wet burlap for 28 days. UHPSFRC properties, including compressive strength (122.93 MPa), tensile strength (8.1 MPa), and modulus of elasticity (41,946 MPa), were evaluated per ASTM C39/C39M and ASTM C1609/C1609M, ensuring compliance with standardized protocols [15,16].

2.2 Experimental Setup

All specimens were tested with the columns oriented horizontally and the beams vertically, a 90-degree rotation from the *in-situ* configuration as presented in Fig. 3. This facilitated the application of the axial column load.

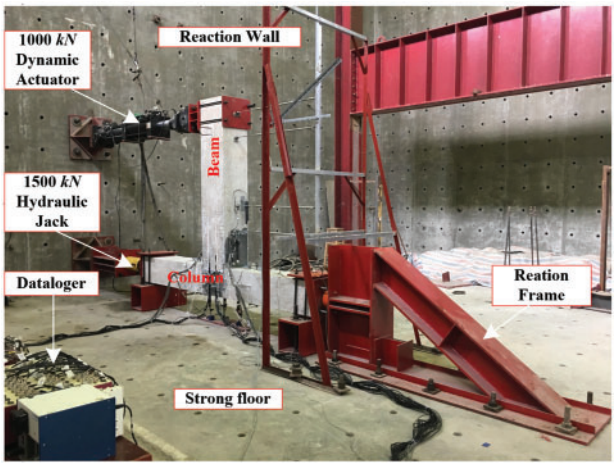

Figure 3: Experimental setup

A 500 kN capacity actuator, capable of ±500 mm displacement, was positioned at the beam end to apply horizontal cyclic shear loading parallel to the reaction frame (Fig. 4a). Separately, a 1500 kN static actuator applied a constant 650 kN axial load to the column head (Fig. 4b). Load cells continuously monitored both axial and shear forces (Fig. 4c). A computer-based data acquisition system recorded data from Linear Variable Differential Transformers (LVDTs) and strain gauges throughout the test. A high-strength steel frame, acting as a reaction frame, was rigidly attached to the reaction floor using ten 33 mm diameter bolts (Fig. 4d). The test setup allowed only rotational displacement at the column ends, enforced by supports and rollers (Fig. 4e). High-strength bolts further secured the column bases to the floor, preventing out-of-plane movement.

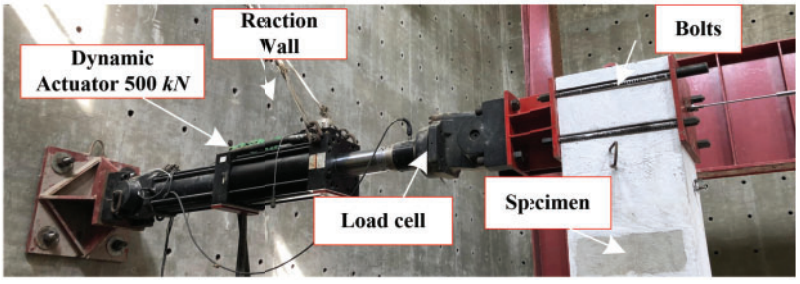

(**a**) Dynamic Actuator

Figure 4: (Continued)

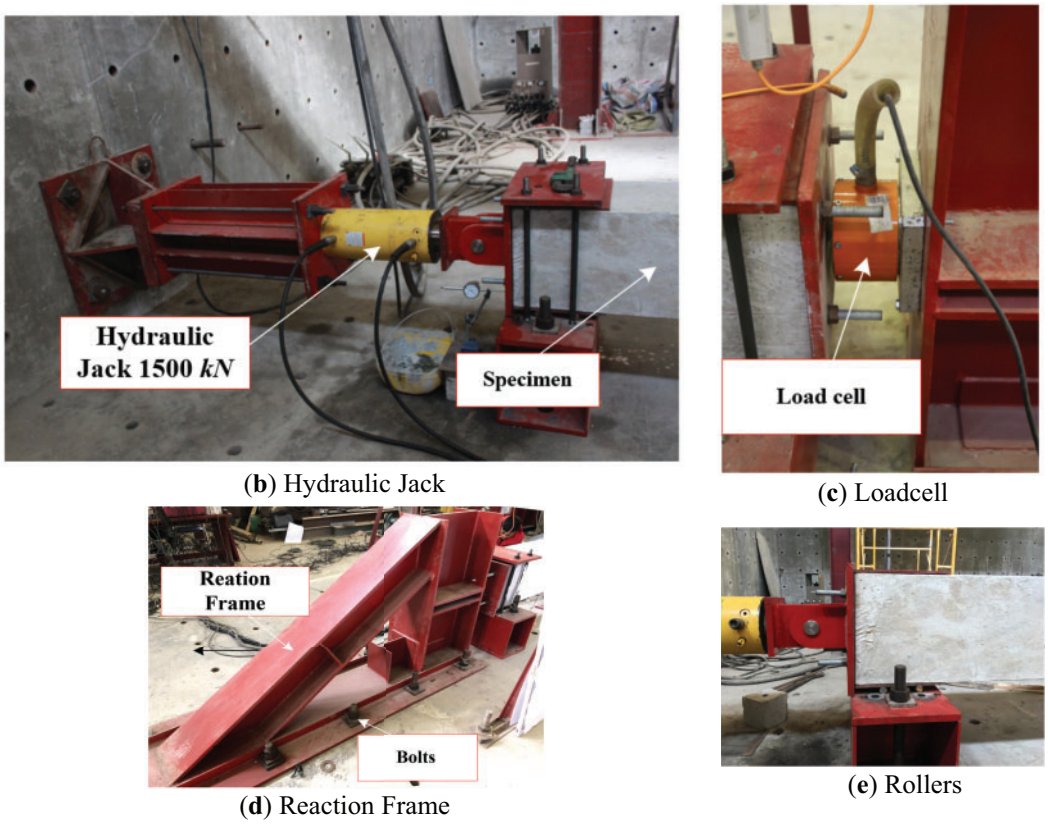

(**b**) Hydraulic Jack (**c**) Loadcell

(**d**) Reaction Frame (**e**) Rollers

Figure 4: Arrangement of test equipment

2.3 LVDT Displacement Transducer Arrangement

The cyclic loading applied to the beam end necessitates the determination of several key parameters: beam-column rotation angle, predicted plastic hinge rotation angle in the beam, column rotation angle, and joint shear deformation. Each specimen was instrumented with 21 symmetrically arranged LVDT displacement transducers. To measure beam-column rotation, four LVDTs (labeled 1, 2, 20, and 21) were vertically mounted on both sides of the beam in a symmetrical arrangement, spaced 500 mm apart (Fig. 5). During beam displacement, one LVDT will extend while the opposite LVDT compresses. The difference in LVDT readings, divided by the 500 mm spacing, yields the relative beam rotation angle. Additionally, two pairs of LVDTs (labeled 3–4 and 5–6) were vertically mounted on each side of the beam to measure the plastic hinge rotation angle in the beam (Fig. 6). These LVDTs were also spaced 500 mm apart, and the plastic hinge rotation angle was calculated using the same method as for the beam-column rotation angle. Column rotation was measured using LVDTs 9 and 11, vertically mounted 600 mm apart along the beam (Fig. 7). The calculation method for column rotation was the same as for the previously described measurements.

Joint shear deformation (γ) was measured using two diagonally mounted LVDTs (Figs. 7 and 8) and calculated as follows:

$$(\mathrm{D} + \delta_2)^2 - (\mathrm{D} + \delta_1)^2 = (\mathrm{h_c} - \mathrm{x})^2 - (\mathrm{h_c} + \mathrm{x})^2 \tag{1}$$

$$\gamma = \frac{(2D + \delta_1 + \delta_1)(\delta_1 - \delta_2)}{4h_c h_b} \tag{2}$$

where: D is the diagonal length; δ_i is the LVDT displacement; h_c and h_b are the LVDT spacings; and x is the horizontal joint displacement.

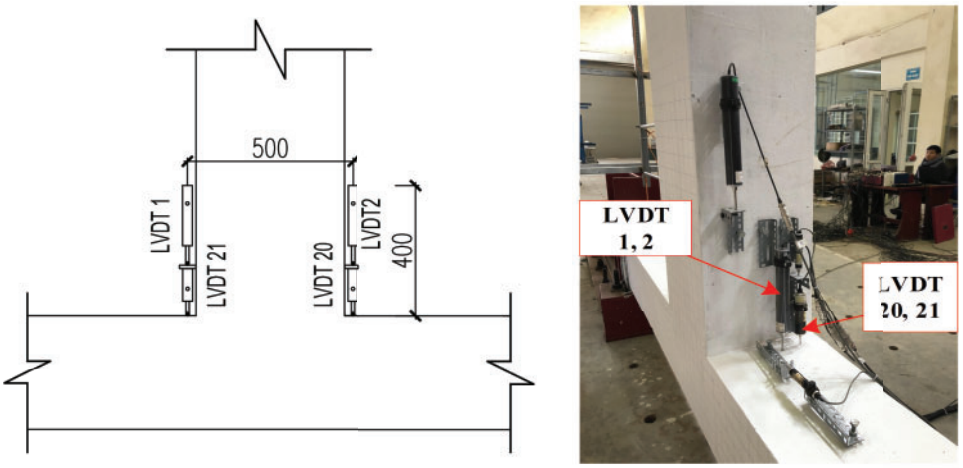

Figure 5: LVDT arrangement for measuring beam-column rotation (Unit: mm)

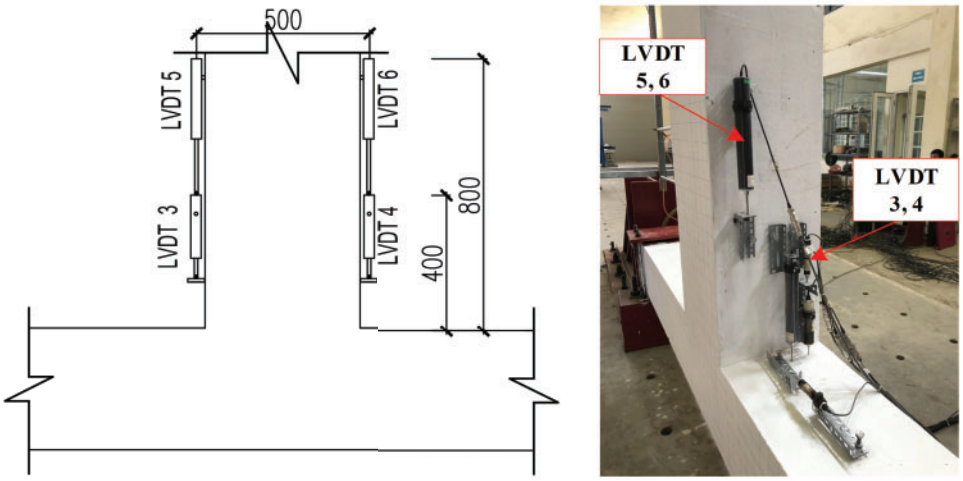

Figure 6: LVDT arrangement for measuring beam plastic hinge rotation (Unit: mm)

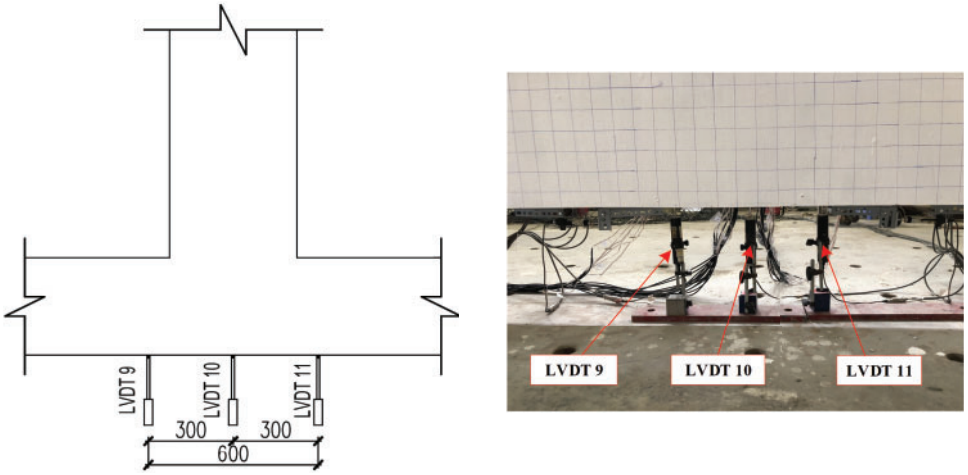

Figure 7: LVDT placement for measuring column rotation (Unit: mm)

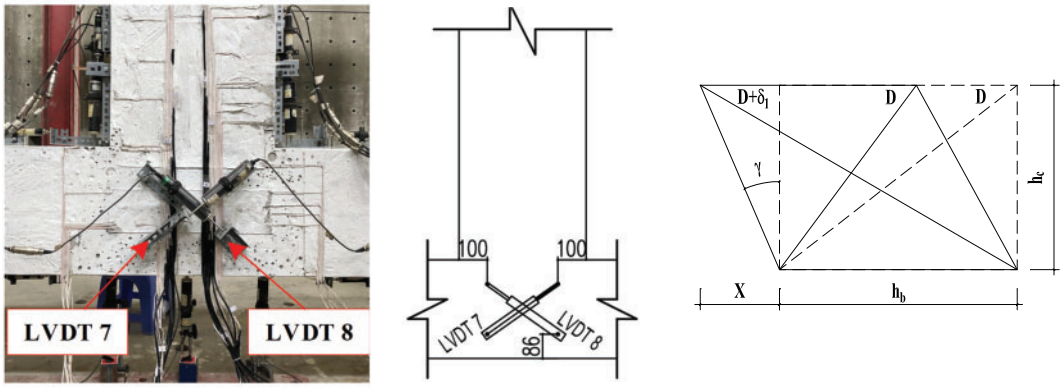

Figure 8: LVDT arrangement for measuring joint deformation (Unit: mm)

2.4 Loading History

Cyclic loading was applied to the specimens with a constant 650 kN axial compressive load (axial load ratio = 0) maintained by a static actuator. The beam-end actuator employed a two-stage loading protocol. The first stage, force-controlled, determined the cracking load. The second stage, displacement-controlled, followed ACI Committee 374 recommendations [27] and established practices [28–30], using a quasi-static loading frequency of 0.01 Hz. Each loading step consisted of three identical displacement cycles at the beam end. The initial displacement amplitude was set to the yield displacement (Δ_y), determined from numerical and experimental analyses. Subsequent displacement amplitudes were: $1\Delta_y$, $1.4\Delta_y$, $1.7\Delta_y$, $2.2\Delta_y$, $2.75\Delta_y$, $3.5\Delta_y$, $4\Delta_y$, $5\Delta_y$, and $6.5\Delta_y$. After twelve cycles, a control cycle with one-third the previous amplitude was introduced (Fig. 9) mitigate stiffness degradation effects. Beam drift was calculated as:

$$\text{Drift} = \frac{\Delta_l}{0.5 l_b} \times 100\% \tag{3}$$

where: Δ_l is the beam-end displacement; and l_b is the beam length.

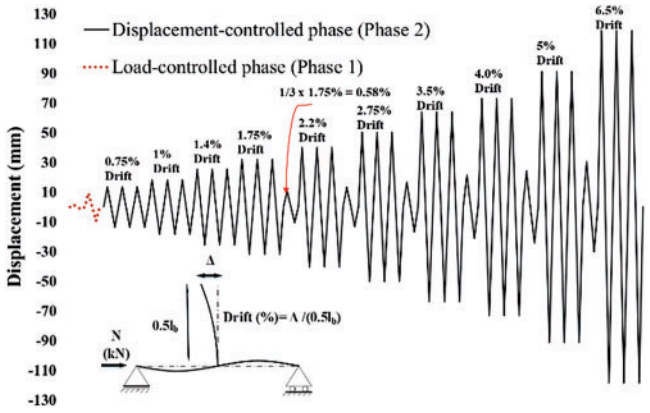

Figure 9: Loading history

3 Experimental Results

3.1 Ductility Analysis

Fig. 10 shows the initial cycle load-displacement hysteresis loops for all three specimens. Determining the yield point in RC structures is challenging due to the nonlinear material behavior (concrete and steel) and the varying inelastic response of different structural components at different load levels.

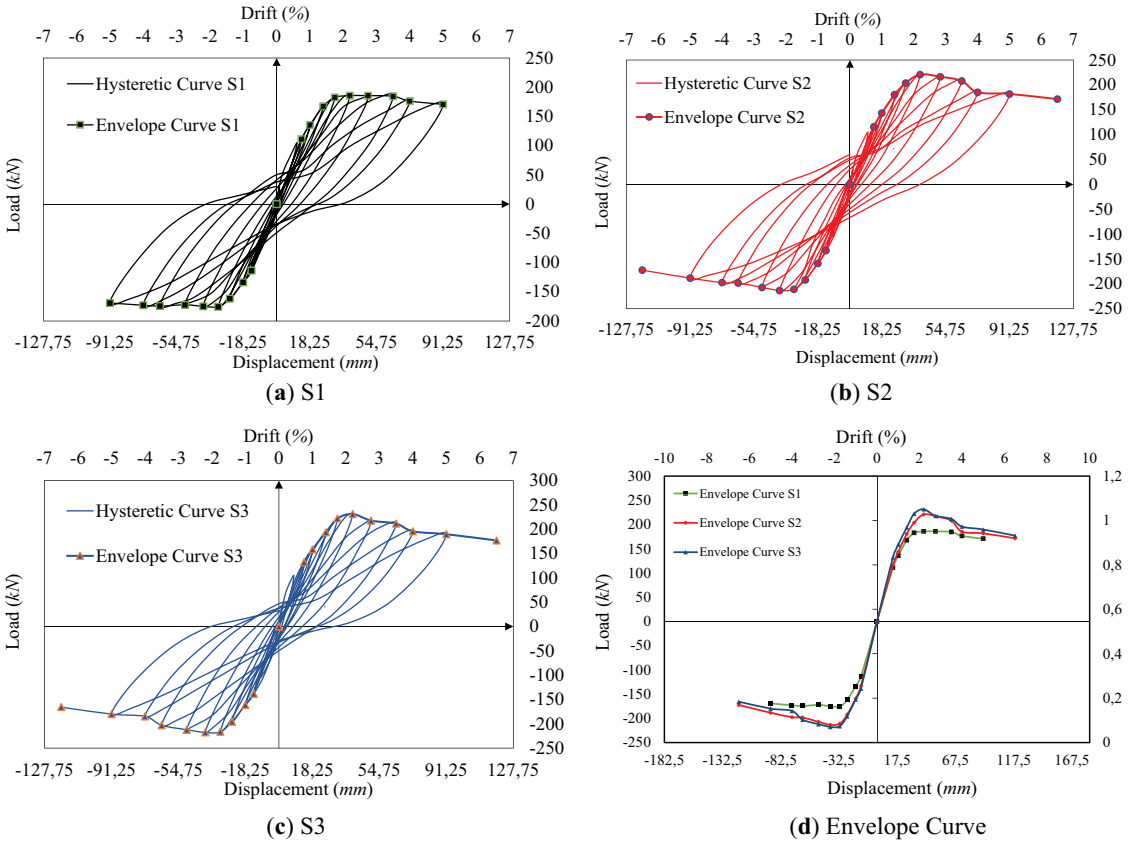

(**a**) S1 (**b**) S2

(**c**) S3 (**d**) Envelope Curve

Figure 10: Load-displacement envelope curves of the test specimens

The ductility factor is calculated as the ratio of the ultimate displacement (Δ_u) to the yield displacement (Δ_y). The ultimate displacement (Δ_u) is defined as the displacement corresponding to 80% of the peak load (P_u) or the onset of steel yielding, whichever occurs first [8]. The yield displacement (Δ_y) is determined by drawing a straight line from the origin to a point on the load-displacement envelope curve corresponding to the initial steel yielding or 75% of the peak load (P_u), whichever is smaller (Fig. 11). This line is then extrapolated to the peak load (P_u). A second line is then drawn from the yield point to intersect the envelope curve such that the areas above and below this line are equal (Fig. 11). The ductility factor (μ) is then calculated as:

$$\mu = \frac{\Delta_u}{\Delta_y} \tag{4}$$

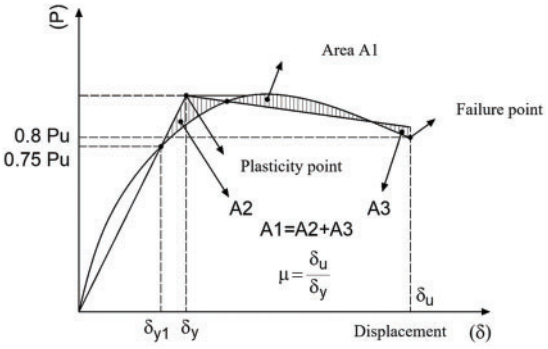

Figure 11: Characteristic points of the idealized load-displacement curve

Table 4, based on the aforementioned calculation method, presents the ductility factors. Despite significant differences in peak loads between the push and pull directions, the ductility factors show minimal variation. This clearly indicates that the UHPSFRC reinforcement enhanced the ductility of the test specimens. Specimen S2 exhibited comparable ductility to the control specimen (S1) in both loading directions; however, Specimen S3 unexpectedly showed a 3.4% increase in ductility in tension but a 4.6% decrease in compression. This suggests that increasing the UHPSFRC length from 450 mm (Specimen S2) to 675 mm (Specimen S3) did not further enhance ductility. In Specimen S3, the yield displacement (Δ_y) ranged from 1.4% drift (25.6 mm) to 2.2% drift (40.15 mm), while the ultimate displacement (Δ_u) was reached during the second cycle at 6.5% drift. After reaching the peak load at 2.2% drift, a significant reduction in load-carrying capacity was observed in the second cycle at 3.5% drift. This is likely due to accumulated damage after reaching the peak load, resulting in a substantial strength reduction and preventing further increases in ductility. The unexpected increase in ductility in tension for Specimen S3 can be attributed to the enhanced tensile strain capacity provided by the thicker UHPSFRC layer, which allowed greater elongation of the steel fibers under tensile forces before crack localization occurred. Conversely, the decrease in ductility in compression likely resulted from localized compressive failure within the UHPSFRC joint region, where the increased thickness may have led to stress concentrations and micro-cracking that reduced the material's ability to deform plastically under compressive loads. This behavior aligns with findings by Chen et al. [14], who observed that higher fiber content in UHPSFRC can enhance tensile ductility but may exacerbate compressive brittleness under cyclic loading due to fiber buckling and matrix crushing. In contrast, Palomo et al. [13] reported consistent ductility improvements in both tension and compression with UHPSFRC, though their study used a lower fiber volume fraction and a different joint configuration, suggesting that the

UHPSFRC thickness and fiber dispersion in Specimen S3 played a critical role in the observed asymmetry. Overall, the average ductility factors for specimens S1, S2, and S3 were relatively consistent at 3.8, 3.7, and 3.8, respectively.

Table 4: Ductility factors for each test specimen

Specimen	P_u (kN)		δ_u (mm)		δ_{y1} (mm)		δ_y (mm)		μ	
	Push	Pull	Push	Pull	Push	Pull	Push	Pull	Push	Pull
S1	185.8	175.7	91.25	91.25	18.25	17	25	23	3.65	3.96
S2	220.8	213.4	104.8	91.25	23	18.25	30	24	3.62	3.8
S3	231.4	217.8	101	102.5	21.7	19	29	25	3.48	4.1

3.2 Stiffness Degradation

The observed stiffness degradation in the RC joints resulted from a complex interplay of factors stemming from the inelastic behavior of the constituent materials under cyclic loading. The deterioration of the bond between the steel reinforcement and the surrounding concrete, evidenced by concrete cracking and spalling, played a significant role in reducing the overall stiffness of the joints. Furthermore, the propagation of cracks, initiated under cyclic loading and exacerbated with increasing drift, progressively weakened the load-carrying capacity of the joints, thereby contributing to the observed stiffness reduction. These phenomena are characteristic of the inelastic behavior of reinforced concrete structures and are particularly pronounced in the joint region, where stress concentrations are typically high. Finally, the separation of concrete from steel, frequently observed in the later stages of cyclic loading, further diminished the load-transfer capability of the joint, causing a more rapid decrease in stiffness.

To quantify this stiffness degradation, the secant stiffness method was employed, which utilizes the load-deformation curve to determine stiffness changes. This method calculates the stiffness at specific loading levels, particularly those corresponding to loading peaks in the cyclic loading sequence, based on the slope of the curve connecting those points. This approach is beneficial when dealing with hysteretic behavior of a non-linear material, offering an accurate representation of the stiffness deterioration compared to methods relying solely on initial elastic stiffness properties. Fig. 12 illustrates the stiffness degradation curves for all three specimens, effectively visualizing the overall stiffness characteristics.

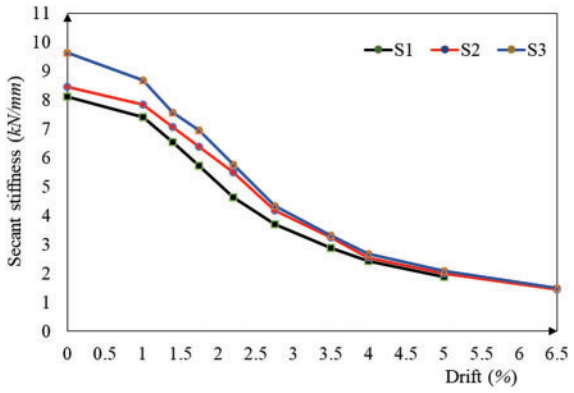

Figure 12: Comparison of secant stiffness for test specimens

As shown in Fig. 13, the UHPC-strengthened specimens (S2 and S3) exhibited significantly higher stiffness than the control specimen (S1) at lower drift levels. This was especially noticeable at a drift of 1.0%, demonstrating the beneficial effect of UHPC reinforcement in enhancing the initial stiffness of the joints. However, as the drift increased from 1.4% to 1.75%, the emergence and propagation of cracks became increasingly apparent in all specimens. This observation resulted in a more rapid rate of stiffness degradation in all specimens due to the aforementioned inelastic material behavior and the subsequent loss of bond between the concrete and the reinforcement.

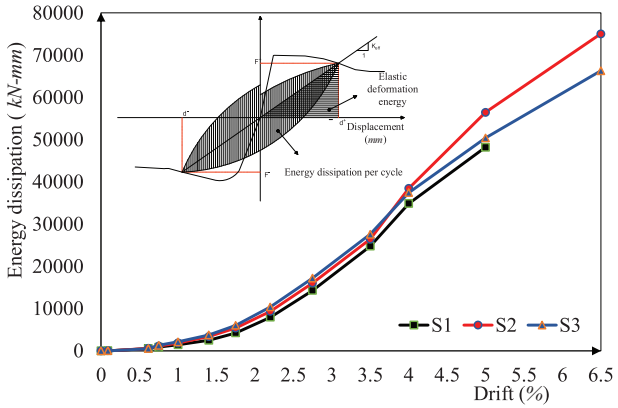

Figure 13: Energy dissipation capacity of test specimens

By the time the specimens reached a drift level of 2.2%, the stiffness of the UHPC-strengthened specimens (S2 and S3) had converged to approximately the same value, indicating a substantial improvement in stiffness (approximately 16%) in comparison to the control specimen (S1). This convergence highlights the strong influence of UHPC in enhancing stiffness, particularly within the inelastic region of material behavior. This improvement in stiffness can be attributed to the inherent properties of UHPC such as enhanced compressive strength, improved ductility, and high tensile strength that significantly increase the overall stiffness of the enhanced joints, thereby mitigating the effects of cracking and spalling and enhancing the joint region's load-bearing capacity. However, at a drift of 4.0%, all specimens experienced significant stiffness degradation (approximately 70% decrease from initial stiffness). This substantial reduction reflects the onset of extensive cracking and material failure within the joint region, indicating that the ultimate load-carrying capacity is being approached, with the ultimate limit of the joint region being approached, ultimately leading to failure. The findings confirm that while UHPC significantly enhanced the initial and mid-range stiffness of the joints, the ultimate limit state was similar for all specimens tested.

3.3 Energy Dissipation Capacity

The energy dissipation capacity of the RC joint specimens was determined by cumulatively summing the hysteretic energy dissipated during each loading cycle. This approach, consistent with the methodology proposed by Priestley [31], utilizes the area enclosed within each load-displacement hysteresis loop as a measure of energy dissipation per cycle (Fig. 13). Fig. 13 illustrates the relationship between drift and energy dissipation for specimens S1, S2, and S3.

A significant enhancement in energy dissipation capacity was observed in the UHPC-strengthened specimens (S2 and S3) compared to the control specimen (S1) at drift levels exceeding 1.0%. This improvement is attributed to the enhanced ductility and energy absorption capabilities of the UHPC material.

At a drift of 2.2%, for instance, specimens S2 and S3 absorbed 3975 kN·m and 4395 kN·m of energy, respectively, representing improvements of 6.5% and 14.67% over the control specimen (S1). This superior energy dissipation capacity highlights the effectiveness of UHPC in mitigating seismic forces and reducing the likelihood of structural damage.

Furthermore, the UHPC-strengthened specimens demonstrated sustained energy dissipation capacity even at higher drift levels. At a drift of 6.5%, specimens S2 and S3 continued to effectively dissipate energy, while the control specimen (S1) reached its ultimate capacity and failed at a significantly lower drift level (5.0%). This observation indicates the enhanced energy dissipation capacity contributed by the UHPC, further highlighting its effectiveness in improving the seismic resilience of RC frame joints. The superior energy dissipation capacity of the UHPC-retrofitted specimens showcases the advantages of utilizing this advanced material to enhance the resilience and safety of RC structures subjected to seismic loads.

3.4 Performance Evaluation of the UHPC-Retrofitted Frame Joint

Joint shear deformation is a critical factor in evaluating the effectiveness of UHPC retrofitting in RC frames subjected to cyclic loading. While current design standards [32,33] prioritize maximum load capacity when focusing solely on internal forces, neglecting deformation considerations, the impact of joint shear deformation on seismic performance remains a subject of ongoing research [34], lacking definitive conclusions. A tri-linear envelope curve (Fig. 14) effectively characterizes the overall frame performance and the localized joint response under cyclic loading. This curve is defined by three key points: Point A, marking the onset of diagonal cracking within the joint; Point B, representing the yield stress of the beam reinforcement; and Point C, signifying the peak load capacity. Beyond Point C, a decrease in joint load capacity occurs due to progressive concrete failure. The slope variations within this tri-linear model effectively capture the changes in secant stiffness throughout the loading process, illustrating the relationship between joint load and deformation.

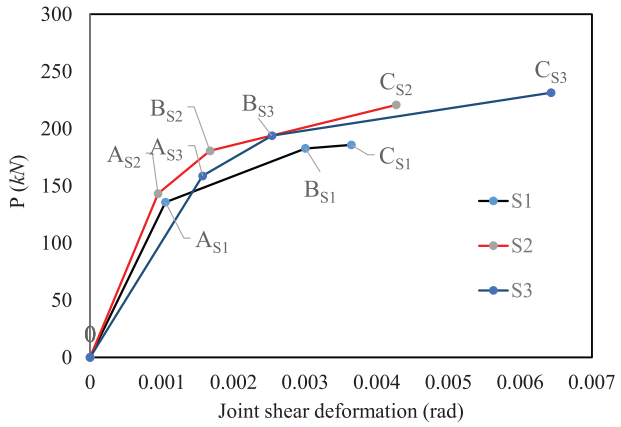

Figure 14: Envelope curve of shear force and displacement

Fig. 14 demonstrates that the UHPC retrofit significantly enhances the secant stiffness of the joints compared to the control specimen (S1) throughout the loading process. At the peak load point (Point C), specimens S2 and S3 exhibit stiffness increases of approximately 14.6% and 43.3%, respectively, over the control specimen. This enhanced stiffness is directly attributed to the UHPC retrofit's influence on the overall joint behavior.

Furthermore, according to FEMA 273 [34], acceptable shear deformation limits for RC structures at collapse ("e" level) and ultimate ("d" level) are 0.01 and 0.005, respectively. As shown in Fig. 14, specimens S2 and S3 satisfy these limits. While specimen S2 maintains a shear deformation approximately 14% below the "d" level limit, specimen S3 slightly exceeds this limit by 22%, yet remains well within the allowable "e" level limit. This confirms the effectiveness of the UHPC retrofit in enhancing the joint stiffness and overall seismic performance of the RC frame joint, even at higher load levels.

4 Conclusions

This experimental study investigated the dynamic behavior, load capacity, and failure mechanisms of UHPC-retrofitted exterior RC frame joints under reversed cyclic loading. Key findings demonstrate:

- Specimen S2 exhibited similar ductility to the control specimen (S1), but Specimen S3 showed lower ductility in the compression direction. This reduction is likely due to accumulated damage within the joint, leading to a significant strength reduction that inhibited further ductility increases. However, the overall average ductility across all three specimens was comparable.
- A significant reduction in normalized principal tensile stresses was observed in the UHPC-retrofitted specimens (S2 and S3) compared to the control specimen (S1), with reductions of 11.6% and 8.2%, respectively, at the maximum load. Concurrently, the UHPC-retrofitted specimens exhibited superior energy absorption and dissipation capabilities, particularly at drift levels exceeding 1.0%, with increases of 6.5% and 14.67% at a drift of 6.5% for S2 and S3 respectively compared to S1.
- All specimens satisfied ACI 374 [14] design criteria for drift limits (3.5% and 2.5%, respectively) under seismic loading, ensuring adequate structural integrity.
- The failure mode of the UHPSFRC-strengthened specimen S2 (450 mm UHPSFRC layer), characterized by desirable flexural failure in the beam, aligns with FEMA 273 [34] criteria for joint performance ("d" and "e" levels), thereby demonstrating the effectiveness of the UHPC retrofit in enhancing the joint's overall seismic performance.

These findings demonstrate the efficacy of UHPC retrofitting in enhancing the strength, ductility, and overall seismic resilience of exterior RC frame joints, offering valuable insights for improving seismic design practices. In practical engineering, UHPSFRC-reinforced joints can be applied to retrofit existing RC buildings in earthquake-prone regions, particularly in developing countries, where they provide a cost-effective solution to enhance structural resilience without requiring extensive reconstruction. A typical application scenario includes strengthening critical beam-column connections in mid-rise buildings to ensure safety and prolong service life under seismic loads.

Acknowledgement: Not applicable.

Funding Statement: The author received no specific funding for this study.

Availability of Data and Materials: The data that support the findings of this study are available from the corresponding author, upon reasonable request.

Ethics Approval: Not applicable.

Conflicts of Interest: The author declares no conflicts of interest to report regarding the present study.

References

1. Buitelaar P. Ultra high performance concrete: developments and applications during 25 years. In: Proceedings of the International Symposium on Ultra High Performance Concrete; 2004 Sep 13–15; Kassel, Germany.

2. Bache HH. Densified cement/ultra-fine particle-based materials. Aalborg, Denmark: Aalborg Portland; 1981.
3. Roy DM, Gouda GR, Bobrowsky A. Very high strength cement pastes prepared by hot pressing and other high pressure techniques. Cem Concr Res. 1972;2(3):349–66. doi:10.1016/0008-8846(72)90075-0.
4. Yudenfreund M, Odler I, Brunauer S. Hardened portland cement pastes of low porosity I. Materials and experimental methods. Cem Concr Res. 1972;2(3):313–30. doi:10.1016/0008-8846(72)90073-7.
5. Setra-AFGC. Ultra high performance fibre-reinforced concretes-interim recommendations. Paris, France: French Association for Civil Engineers; 2002. (In French).
6. Van Zijl GP, Wittmann FH, Oh BH, Kabele P, Toledo Filho RD, Fairbairn EM, et al. Durability of strain-hardening cement-based composites (SHCC). Mater Struct. 2012;45(10):1447–63. doi:10.1617/s11527-012-9845-y.
7. Wille K, Kim DJ, Naaman AE. Strain-hardening UHP-FRC with low fiber contents. Mater Struct. 2011;44(3):583–98. doi:10.1617/s11527-010-9650-4.
8. Wille K, Naaman AE, El-Tawil S, Parra-Montesinos GJ. Ultra-high performance concrete and fiber reinforced concrete: achieving strength and ductility without heat curing. Mater Struct. 2012;45(3):309–24. doi:10.1617/s11527-011-9767-0.
9. Meng L, Zhang C, Wei J, Li L, Liu J, Wang S, et al. Mechanical properties and microstructure of ultra-high strength concrete with lightweight aggregate. Case Stud Constr Mater. 2023;18:e01745.
10. Kim S, Shin J, Kim W. Assessing the seismic performance of exterior precast concrete joints with ultra-high-performance fiber-reinforced concrete. Int J Concr Struct Mater. 2024;18(1):10. doi:10.1186/s40069-023-00646-9.
11. Nadir W, Ali AY, Jawdhari A, Kadhim MMA, Majdi A. Cyclic behavior of UHPC corner beam-column joints under bi-directional bending. Structures. 2024;60(2):105857. doi:10.1016/j.istruc.2024.105857.
12. Roth MJ, Boone NR, Kinnebrew PG, Davis JL, Rushing TS. Development of new protective solutions to counter emerging and adaptive threats. In: Proceedings of the 26th Army Science Conference; 2008 Dec 1–4. Vicksburg, MS, USA: US Army Engineer Research and Development Center; 2008. p. 1–4.
13. Palomo IRI, Frappa G, de Almeida LC, Trautwein LM, Pauletta M. Analytical and numerical models to determine the strength of RC exterior beam-column joints retrofitted with UHPFRC. Eng Struct. 2024;312(2):118244. doi:10.1016/j.engstruct.2024.118244.
14. Chen L, Xu J, Wu H. Cyclic behavior of UHPSFRC-strengthened RC joints: influence of fiber content and joint detailing. Constr Build Mater. 2023;405:133245.
15. ASTM C39/C39M-24. Standard test method for compressive strength of cylindrical concrete specimens. West Conshohocken, PA, USA: ASTM International; 2024 [cited 2025 Feb 27]. Available from: https://store.astm.org/c0039_c0039m-24.html.
16. ASTM C1609/C1609M-19a. Standard test method for flexural performance of fiber-reinforced concrete (using beam with third-point loading). West Conshohocken, PA, USA: ASTM International; 2019 [cited 2025 Feb 27]. Available from: https://store.astm.org/c1609_c1609m-19a.html.
17. Sleiman E, Ferrier E, Michel L, Saidi M. Seismic behavior of masonry-infilled reinforced concrete frames strengthened using ultra-high performance concrete diagonal strips. Structures. 2024;59(1):105790. doi:10.1016/j.istruc.2023.105790.
18. Zeng JJ, Hao ZH, Sun HQ, Zeng WB, Fan TH. Durability assessment of ultra-high-performance concrete (UHPC) and FRP grid-reinforced UHPC plates under marine environments. Eng Struct. 2025;323(Part B):119313. doi:10.1016/j.engstruct.2024.119313.
19. Hung CC, Lin CC, Do TDD. Seismic rehabilitation of RC frames with innovative precast U-shaped UHPC jackets: experimental evaluation and computational simulation. Eng Struct. 2024;318(3):118746. doi:10.1016/j.engstruct.2024.118746.
20. Cao XY, Feng DC, Wang CL, Shen D, Wu G. A stochastic CSM-based displacement-oriented design strategy for the novel precast SRC-UHPC composite braced-frame in the externally attached seismic retrofitting. Compos Struct. 2023;321(8):117308. doi:10.1016/j.compstruct.2023.117308.
21. Clyde C, Pantelides CP, Reaveley LD. Performance-based evaluation of exterior reinforced concrete building joints for seismic excitation. Berkeley, CA, USA: Pacific Earthquake Engineering Research Center; 2000.

22. Hertanto E. Seismic assessment of pre-1970s reinforced concrete structures [master's thesis]. Christchurch, New Zealand: University of Canterbury; 2005.
23. Pantelides CP, Clyde C, Reaveley LD. Performance-based evaluation of reinforced concrete building exterior joints for seismic excitation. Earthq Spectra. 2002;18(3):449–80. doi:10.1193/1.1510447.
24. Genesio G. Seismic assessment of RC exterior beam-column joints and retrofit with haunches using post-installed anchors [dissertation]. Stuttgart, Germany: Institut für Werkstoffe im Bauwesen der Universität Stuttgart; 2012.
25. Guo R, Zhang L, Wang P. Advances in UHPSFRC for seismic-resistant structures: a focus on joint behavior. J Struct Eng. 2024;150(5):04024012.
26. Pham D, Le T, Hoang N. Cost-effective seismic retrofitting of RC structures in developing countries using UHPC: challenges and opportunities. Sustain Cities Soc. 2023;98:104832.
27. ACI Committee 374. Acceptance criteria for moment frames based on structural testing and commentary: an ACI standard. Farmington Hills, MI, USA: American Concrete Institute; 2005.
28. Chun SC, Lee SH, Kang TH, Oh B, Wallace JW. Mechanical anchorage in exterior beam-column joints subjected to cyclic loading. ACI Struct J. 2007;104(1):102–11.
29. Ghobarah A, El-Amoury T. Seismic rehabilitation of deficient exterior concrete frame joints. J Compos Constr. 2005;9(5):408–16. doi:10.1061/(ASCE)1090-0268(2005)9:5(408).
30. Hakuto S, Park R, Tanaka H. Seismic load tests on interior and exterior beam-column joints with substandard reinforcing details. ACI Struct J. 2000;97(1):11–25.
31. Priestley MJN. Displacement-based seismic assessment of reinforced concrete buildings. J Earthq Eng. 1997;1(1):157–92. doi:10.1080/13632469708962365.
32. Naaman AE, Wille K. The path to ultra-high performance fiber reinforced concrete (UHP-FRC): five decades of progress. In: Proceedings of the 3rd International Symposium on UHPC and Nanotechnology for High Performance Construction Materials; 2012 Mar 7–9; Kassel, Germany; p. 3–15.
33. Pantazopoulou SJ, Bonacci JF. On earthquake-resistant reinforced concrete frame connections. Can J Civ Eng. 1994;21(2):307–28. doi:10.1139/l94-032.
34. Building Seismic Safety Council. FEMA 273/274—NEHRP guidelines for the seismic rehabilitation of buildings, vol. I—guidelines, vol. II—commentary. Washington, DC, USA: Federal Emergency Management Agency; 1997.